

The Role of Oxygen Transfer in Oxide Heterostructures on Functional Properties

Zachary Corey, Henry H. Han, Kyeong Tae Kang, Xuejing Wang, Rebecca A. Lalk, Binod Paudel, Pinku Roy, Yogesh Sharma, Jinkyong Yoo, Quanxi Jia,* and Aiping Chen*

A variety of mechanisms are reported to play critical roles in contributing to the high carrier/electron mobility in oxide/SrTiO₃ (STO) heterostructures. By using La_{0.95}Sr_{0.05}TiO₃ (LSTO) epitaxially grown on different single crystal substrates (such as STO, GdScO₃, LaAlO₃, (LaAlO₃)_{0.3}(Sr₂AlTaO₆)_{0.7}, and CeO₂ buffered STO) as the model systems, the formation of a conducting substrate surface layer (CSSL) on STO substrate is shown at relatively low growth temperature and high oxygen pressure (725 °C, 5×10^{-4} Torr), which contributes to the enhanced conductivity of the LSTO/STO heterostructures. Different from the conventional oxygen vacancy model, this work reveals that the formation of the CSSL occurs when growing an oxide layer (LSTO in this case) on STO, while neither annealing nor the growth of an Au layer alone at the exact same growth condition generates the CSSL in STO. It demonstrates that the oxide layer actively pulls oxygen from STO substrate at given growth conditions, leading to the formation of the CSSL. The observations emphasize the oxygen transfer across film/substrate interface during the synthesis of oxide heterostructures playing a critical role in functional properties.

achieved by interfacing two insulating oxides have attracted great attention in the past decade.^[3–10] Different conduction mechanisms including polar catastrophe (interface),^[5,10,11] strain,^[12–14] intermixing (doping),^[3,8,15–17] and oxygen vacancy (defect)^[18–21] have been proposed to explain such phenomenon. For example, carriers at the substrate–film interface (interface), bulk part of the film (film) and the surface layer of the substrate near the substrate–film interface (substrate surface layer) can all contribute to the effective conductivity of the samples. Polar catastrophe is a well-established model to explain the high conductivity at the interface between LaAlO₃ and SrTiO₃ (LAO/STO).^[5,11,20] High mobility has also been reported when LaTiO₃ (LTO) and La_{1-x}Sr_xTiO₃ (LSTO) are grown on SrTiO₃ (STO)^[8,14,16,22] and KTaO₃ (KTO).^[6] LTO is a polar perovskite like LAO, and as such, polar catastrophe

mechanisms of this system are assumed to follow similarly to that of LAO/STO heterostructures.^[5,11,20] However, unlike LAO, which is a band insulator, LTO is a Mott insulator that shows an insulator–metal transition when doped with Sr²⁺ in polycrystalline bulk and epitaxial thin films. This allows the 3d¹ configuration to approach 3d⁰ and may also result in the observed metallic behavior as reported in LSTO films on substrates such as (LaAlO₃)_{0.3}(Sr₂AlTaO₆)_{0.7} (LSAT).^[17,23]

In addition, defects such as oxygen vacancy (OV) in the STO substrate are another factor which could affect the electric conductivity in STO-based heterostructures. The formation of OV in STO substrate is directly controlled by growth temperature and oxygen pressure as reported in different oxide/STO heterostructures.^[5,15,18,20,21,23–28] Enhanced conductivity is observed for these heterostructures grown (and STO single crystals annealed) in temperatures greater than 750 °C, at oxygen pressures lower than 10^{−5} Torr or a combination of both.^[29] For example, OVs can be introduced by reducing the STO substrate with pre-substrate annealing (PSA) at 750 °C and 10^{−6} Torr.^[28] Spinelli, et al. reported highly conductive STO crystals annealed at 10^{−9} Torr and 700 °C.^[29] Schneider et al. found substantial oxygen transfer from STO substrates to oxide films while studying the diffusion of isotope ¹⁸O at the conditions of 750 °C and 1 × 10^{−8} Torr.^[19] Edmondson et al. observed STO substrate reduction at 10^{−10} ~ 10^{−7} Torr and 700 °C.^[20] Therefore, the formation of OV near the STO surface or the diffusion of oxygen out


1. Introduction

Strain, defects, and interfaces play critical roles in controlling functional properties in a variety of oxide heterostructures and nanocomposites.^[1,2] High carrier mobility and high conductivity

Z. Corey, P. Roy, Q. Jia
Department of Materials Design and Innovation
University at Buffalo – The State University of New York
Buffalo, NY 14260, USA
E-mail: qxjia@buffalo.edu

H. H. Han,^[†] K. T. Kang, X. Wang, R. A. Lalk, B. Paudel,
P. Roy, Y. Sharma, J. Yoo, A. Chen
Center for Integrated Nanotechnologies (CINT)
Los Alamos National Laboratory
Los Alamos, NM 87545, USA
E-mail: apchen@lanl.gov

B. Paudel
Department of Physics
New Mexico State University
Las Cruces, NM 88001, USA

 The ORCID identification number(s) for the author(s) of this article can be found under <https://doi.org/10.1002/admi.202101867>.

^[†]Present address: Energy and Environment Directorate, Pacific Northwest National Laboratory, Richland, Washington 99352, USA

DOI: 10.1002/admi.202101867

from STO is driven by the relatively higher temperature (e.g., $>750^{\circ}\text{C}$) and low oxygen pressure (e.g., $<1 \times 10^{-5}$ Torr). Lower temperatures or higher oxygen pressures often result in insulating or significantly lowered conductivity. Post-growth annealing in oxygen rich environments can produce highly resistive films by significantly reducing the OV's.^[3,5,12,15,16,20,21,30]

Except OVs directly induced by growth conditions (relatively high temperature/low oxygen pressure), there are other reduction mechanisms including Ar-ion bombardment,^[31] plasma plume,^[27] and unintentional chamber contamination.^[25] UV radiation from the plasma plume was found to increase OV formation as compared to the STO substrates in the same vacuum condition without UV radiation,^[26] and plume species were also observed to trigger redox reactions for LAO/STO heterostructures.^[27] Creating OVs in STO substrates has also been investigated by reducing STO substrate with the use of Ar-ion bombardment for LAO/STO films.^[21] The Hall mobility of Ar-ion bombarded STO was found to be the same as LAO/STO films grown at low oxygen pressures, and low oxygen pressure annealed STO substrate alone showed nearly the same sheet resistivity as LAO/STO prepared under the same growth conditions.

Although conduction mechanisms based on polar catastrophe and OV in LAO/STO systems are well studied,^[5,15,20,21,32] the origin of OV is less clear.^[6,8,10,14,19,20,33] The generation of OV is often believed to be due to the low oxygen growth pressure at high growth temperatures.^[19–21] However, the oxygen transfer between the oxide substrate and oxide layer could be linked to OV origin.^[19,20,33] In this work, we have used $\text{La}_{0.95}\text{Sr}_{0.05}\text{TiO}_3$ (LSTO) films as a platform to reveal the role of oxygen transfer during heterostructure synthesis on conductivity of the systems. We selected LSTO because it 1) has a similar structure to STO, and 2) has significant lower mobility than STO. We study the roles of substrate, processing oxygen pressure, thickness and heterointerface on the conductivity of LSTO based heterostructures. We have isolated the contributions from the film layer, substrate, and film-substrate interface separately, and concluded that the enhanced conductivity in our LSTO/STO heterostructures is due to the formation of a conducting substrate surface layer (CSSL) near STO top surface. To understand the formation mechanism of the CSSL, Au/STO reference samples were synthesized at the same growth conditions as LSTO/STO. Interestingly, our results demonstrated that this CSSL is not directly driven by processing condition alone (It is well accepted that STO losses oxygen at high temperature and low oxygen processing conditions), rather it is formed because the growth of the oxide layer (LSTO in this case) actively pulls oxygen from STO substrate at the given growth condition. Our results offer a new understanding of OV formation during thin film growth via oxygen transfer mechanisms and can be applied for the growth of a variety of complex oxide films.

2. Results and Discussion

As shown in Figure 1a, the shifting of (002) diffraction angle of LSTO peaks on different substrates indicates different levels of out-of-plane strain. This is expected given the lattice mismatch between the bulk LSTO ($a \sim 3.958 \text{ \AA}$)^[23,34] and the substrates LAO ($a = 3.792 \text{ \AA}$, -4.32%), LSAT ($a = 3.868 \text{ \AA}$, -2.53%), STO

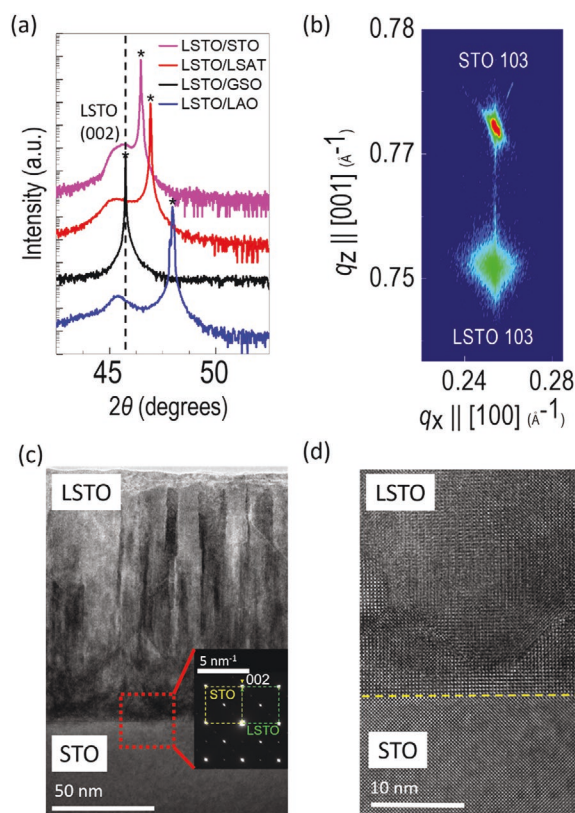


Figure 1. a) θ - 2θ scans of 28 nm LSTO films grown on different substrates around diffractions of (110) GSO, (001) LSAT, (001) LAO and (001) STO. Substrate peaks are marked as * and the dashed line indicates the location of (002) LSTO with negligible strain. b) RSM for 122 nm LSTO film on STO near diffractions of (103) of the film and the substrate. c) Transmission electron microscopy (TEM) image of 122 nm LSTO/STO heterostructure, where the inset shows selected area electron diffraction pattern. d) High-resolution TEM (HRTEM) image across the interface between LSTO and STO.

($a = 3.905 \text{ \AA}$, -1.39%) and GSO ($a = 3.961 \text{ \AA}$, 0.08%). The strain along the c -axis for LSTO/LSAT, LSTO/LAO, LSTO/STO and LSTO/GSO is 0.72% , 0.65% , 0.26% and nearly strain free, respectively. The lattice mismatch between the LSTO and the GSO is negligible and leads to the overlap of (002) LSTO diffraction with the GSO substrate peak. Figure 1b shows a typical reciprocal space map (RSM) near STO (103) peak. It shows that the LSTO film is probably fully strained in-plane to the STO substrate. The epitaxial relationships based on X-ray diffraction (XRD) analysis can be described as $(001)_{\text{LSTO}} \parallel (001)_{\text{Substrate}}$ and $[110]_{\text{LSTO}} \parallel [110]_{\text{Substrate}}$. The HRTEM image in Figure 1d shows the sharp interface of the LSTO film on the STO substrate. The columnar structure is seen above a few tens of nanometers, indicating that the growth deviates from the 2D epitaxial growth. The formation of zig-zag or pyramid-like topological features could be due to the lower surface energy, which is also reported in TiO_2 .^[35] It is noted that the diffraction pattern shown in the inset of Figure 1c also confirms the epitaxial growth of the film and the orientation relationship between the film and the substrate.

Figure 2a shows the ρ - T curves for 28 nm LSTO films on different substrates, where the overall temperature-dependent resistivity for LSTO on LAO, LSAT and GSO is similar to the

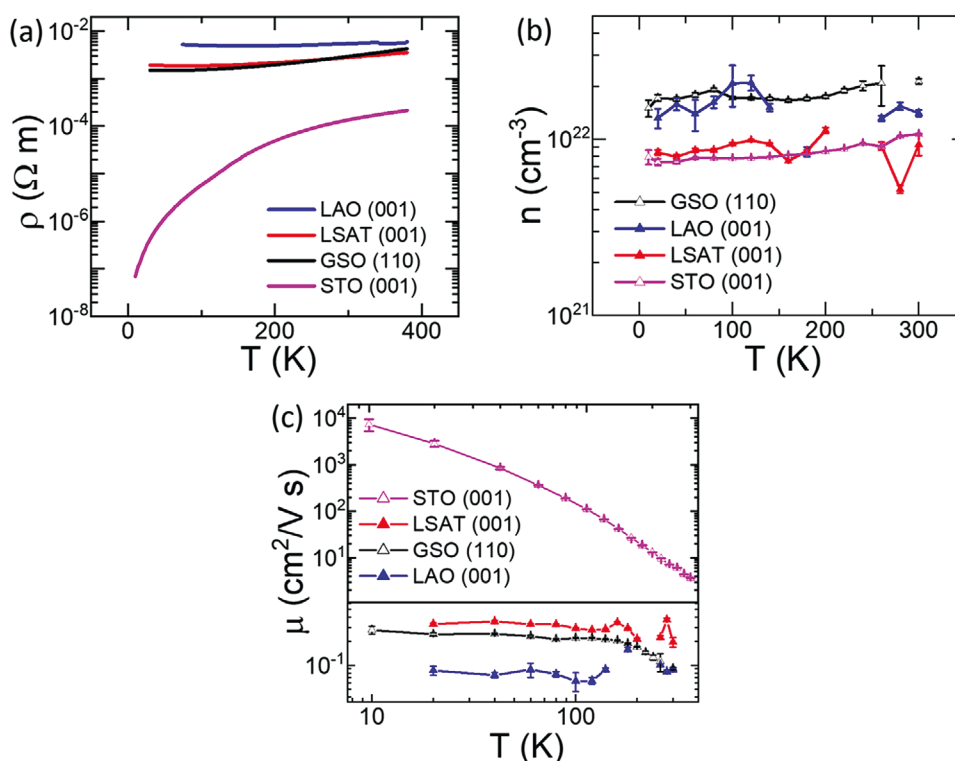


Figure 2. Substrate materials dependent Hall measurements for LSTO films grown at 5×10^{-4} Torr of oxygen. a) Resistivity vs. temperature (ρ - T) where the strain along the c -axis is indicated accordingly, b) Carrier concentration vs. temperature (n - T), c) Mobility vs. temperature (μ - T) for these films on different substrates.

reported results.^[17,23,36,37] A resistivity value $\approx 10^{-4}$ – 10^{-3} Ω cm for our LSTO films (on LAO, LSAT and GSO) grown at an oxygen pressure of 5×10^{-4} Torr is consistent with the reported data.^[17,23] However, different from previous reported p -type conductivity of $\text{La}_{1-x}\text{Sr}_x\text{TiO}_3$ ($0 < \text{Sr} < 0.1$) films, LSTO films in this work grown on different substrates exhibit n -type conductivity. The mobility of the LSTO films ranges from 0.1 to ~ 1 $\text{cm}^2 \text{V}^{-1} \text{s}^{-1}$ and the carrier concentration is about 10^{22}cm^{-3} (as shown in Figure 2b,c). The growth of LSTO films at low oxygen partial pressure in our experiment may promote the formation of n -type conductivity due to OV, similar to the reported results for STO and TiO_2 .^[4] Since these three different substrate materials are insulating even subjected to the low oxygen pressure environment at high growth temperature, the resistivity illustrated in Figure 2a should be from the LSTO films only.

Interestingly, the LSTO/STO heterostructure shows a much lower resistivity as shown in Figure 2a, and this significant change cannot be explained by the lattice strain. Figure 2b shows that carrier concentration is approximately the same for all samples. On the other hand, the LSTO/STO stack exhibits much higher mobility as shown in Figure 2c. It is also noted that the high mobility of LSTO/STO stack and its temperature dependence of μ - T characteristic are similar to the results of an amorphous LAO layer on STO substrate and reduced STO.^[18,21,31,38] Since the resistivity of reduced STO is one magnitude lower than that of LSTO at room temperature and 3–4 orders of magnitude lower at 10 K, it is clear that the resistivity in LSTO/STO stack is dominated by the more conductive STO substrate and/or the LSTO/STO interface. To exclude the

interfacial contribution from the LSTO/STO heterostructure, we also inserted a CeO_2 (5–10 nm) layer between LSTO and STO. Our experimental results showed that CeO_2 interlayer has no obvious effect on the mobility and slightly reduces the carrier concentration below 200 K (Figure S1, Supporting Information). This clearly indicates that the interface between the LSTO and the STO is not critical to achieving enhanced conductivity, different from the LAO/STO case.^[5]

We have varied the oxygen pressure during the growth of LSTO films on STO and observed the effects on conductivity. Figure 3 shows the Hall measurement results of LSTO films on STO grown at different oxygen partial pressure. It has been reported that oxygen partial pressure during the film growth has a strong effect on the overall resistivity of the materials studied.^[3,5,15,18,20,21,23,27] Our results showed the similar trend. Specifically, samples grown at a higher oxygen pressure shows a higher resistivity than samples grown at lower oxygen pressures (Figure 3a). For example, the LSTO film (grown at 5×10^{-4} Torr) on STO exhibits a resistivity of $\rho \approx 2 \times 10^{-5} \Omega$ cm at room temperature, which are two orders of magnitude lower than that of the sample grown at 5×10^{-3} Torr. The temperature-dependent carrier density and mobility shown in Figures 3b,c demonstrated that both decreased carrier concentration and mobility with increasing oxygen pressure during film growth could contribute to the increased resistivity at a given temperature. However, the significantly reduced carrier concentration dominates the increased resistivity at higher temperatures because the mobility is not dramatically affected by changing the oxygen pressure during the film growth. At lower temperatures such as 10 K, however, the

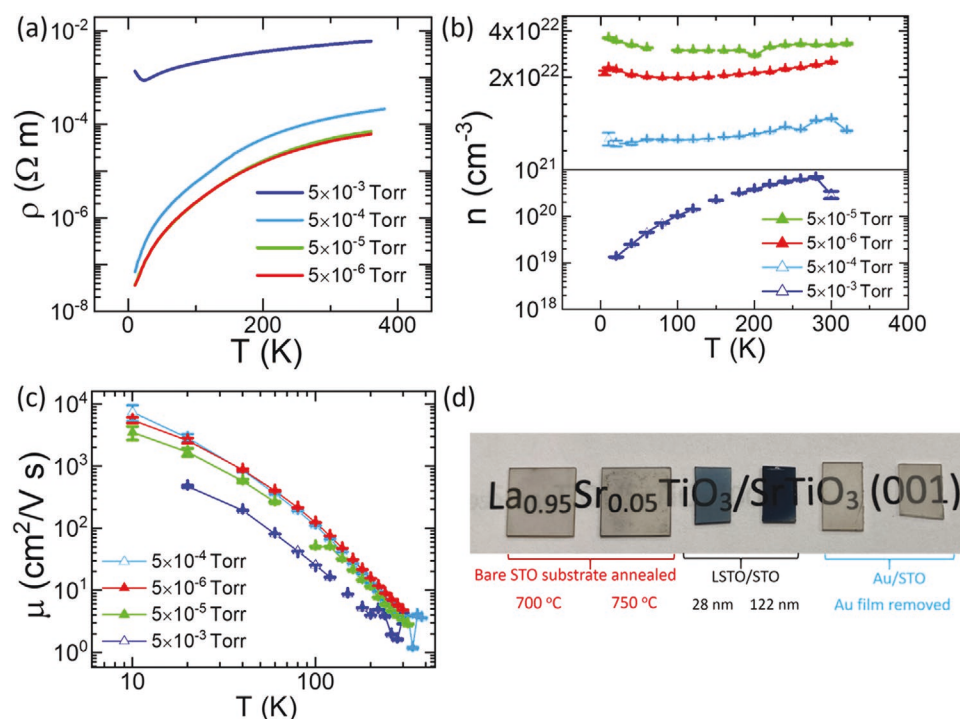


Figure 3. Temperature-dependent a) resistivity, b) carrier concentration, and c) mobility of LSTO films on STO grown in different oxygen partial pressure. (d) Photos of bare STO substrates (left two square samples) annealed in oxygen ($<5 \times 10^{-4}$ Torr) at 700 °C and 750 °C, LSTO/STO heterostructures (middle two dark color samples), and Au/STO heterostructures after removing Au films.

mobility can still show one magnitude difference resulting from the oxygen pressure used in our experiments. This is reasonable since high oxygen partial pressure reduces the OV concentration as well as the OV related carriers. One could clearly use such a strategy, i.e., oxygen pressure during film growth, to manipulate the carrier mobility and concentration, and therefore the effective conductivity of the heterostructure stack.

Figure 3d shows the optical photos of bare STO substrates treated under the similar growth conditions used for the LSTO film growth and the LSTO/STO heterostructures with different LSTO film thicknesses. These bare STO substrates were annealed at an oxygen pressure of 5×10^{-4} Torr and a temperature of 700 or 750 °C for 30 min. As can be seen from the photos, annealed STO substrates under such conditions are still transparent and transport measurements confirm the insulating behavior from both treated substrates. We, however, have found that STO substrate changes to gray/blue color when the annealing is carried out at an oxygen pressure of 5×10^{-4} Torr at a temperature above 800 °C. These experimental results clearly illustrated that annealing of STO in a reducing environment (5×10^{-4} Torr, 700–750 °C, 30 min) alone is not sufficient to change a transparent and highly insulating STO substrate to conductive and/or a different color. However, the LSTO/STO stacks with 28 nm and 122 nm LSTO show distinct light blue and dark blue color. As LSTO film has a bandgap of about ≈ 3.72 eV (Figure S2, Supporting Information, Tauc plot and photos of LSTO film on MgO) and is transparent, the blue color of LSTO/STO stacks should come from reduced STO substrate. Our results are consistent with reported color changes of reduced STO.^[39] We therefore propose that growing an oxygen deficient

oxide layer on top of STO in a suitable reducing environment can promote oxygen transfer from STO substrate to the oxygen deficient film. This is consistent with the oxygen sponge effect, which shows STO substrate can be a source of oxygen for oxide films grown at low oxygen pressure.^[28] Therefore, we propose that the STO substrate surface, contacting with the oxide film, suffers from a redox process during the oxide film growth in an oxygen deficient environment. This redox process produces a thin surface layer right on the top of the STO substrate that is oxygen deficient and highly conductive. Laser plume has also been reported to reduce the STO substrate during the PLD process and make the STO more conductive.^[26] To exclude such an effect in our case, we grew Au films under the same growth condition (as outlined above) on STO substrates. The STO substrates as shown in Figure 3d, after removing the Au film, are insulating and transparent. Therefore, the exposure to the laser plume during the film growth has a minor effect in our case. This designed experiment also supports our hypothesis that the growth of oxide films in a reducing environment pulls oxygen from STO substrates, while the growth of a non-oxide stable metal film such as Au and annealing alone at the same growth conditions do not induce oxygen transfer from STO substrate.

To explore the effect of LSTO layer thickness on the formation of conducting substrate surface layer (CSSL), LSTO/STO heterostructures with different LSTO thicknesses have been grown and measured. Figure 4a shows the ρ - T curves of films ranging from 18 to 122 nm and the resistivity is calculated based on the LSTO film thickness. It is seen that the ρ - T curves are not a strong function of film thickness. If the STO substrate is highly resistive or the resistivity of the LSTO film is far smaller than that of the

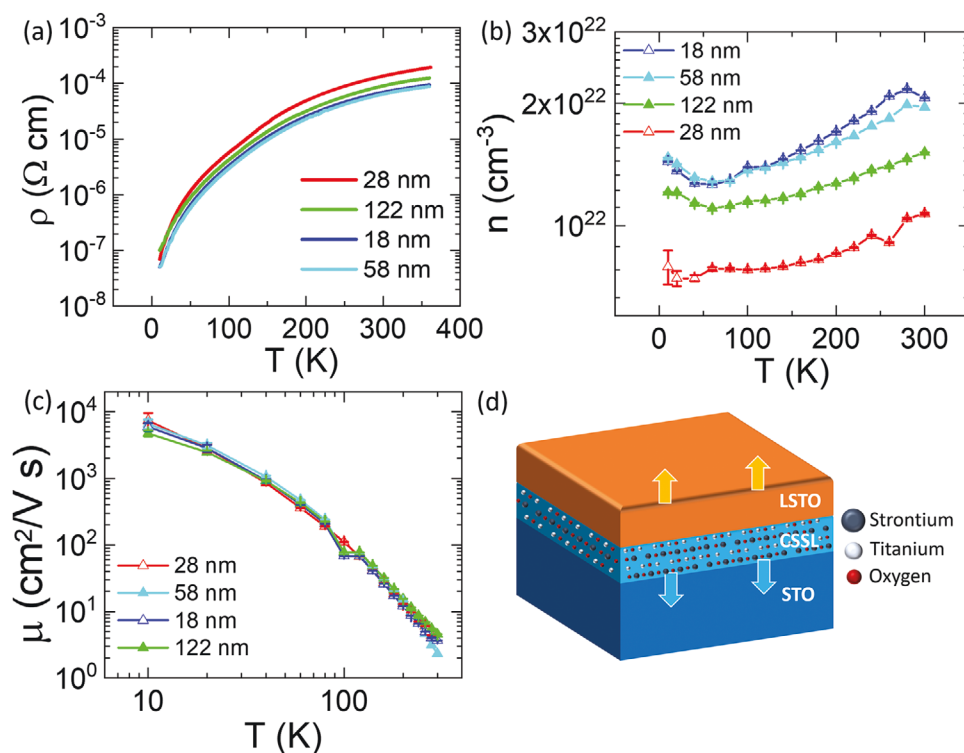


Figure 4. Temperature-dependent a) resistivity, b) carrier concentration, and c) mobility of LSTO/STO stacks with different LSTO film thickness. d) An illustration of increasing the conducting substrate surface layer (CSSL) with increasing film thickness.

substrate, one could simply conclude that the film layer contributes to the measured conductivity. In our case, the experimental results have shown that the STO substrate, subjected to a thermal cycle at high temperature in a low oxygen pressure, exhibits a much lower resistivity which is 2–4 magnitude lower than that of LSTO films. Therefore, the ρ - T curves shown in Figure 4a should be controlled by the CSSL in STO. To show the LSTO thickness independent conductivity of the LSTO/STO heterostructures, the CSSL must also increase in thickness with the growth of LSTO films (Figure 4b,c). As we have discussed earlier, the LSTO film grown on STO in a relatively low oxygen pressure can pull oxygen out from the STO and leave OV in the STO substrate. It is expected that the CSSL thickness increases with the growing thicker LSTO layer as it creates more OV near the STO interface. As schematically illustrated in Figure 4d, the CSSL increases in thickness when the LSTO film grows thicker. Understanding the existence and the origin of this CSSL becomes relevant since STO substrate offers the ability to provide oxygen to oxidize the film during the growth in low oxygen pressures.^[19,27,28] As one of the most commonly used substrates for the growth of multifunctional complex metal oxide films, STO itself could be responsible for some other reported exotic phenomena.

3. Conclusion

In this study, we have examined the effects of substrate materials, film thickness, and oxygen pressure for LSTO films to isolate the contributions of LSTO film, film-substrate interface, and substrate on the conductivity of the heterostructures.

LSTO/STO stack shows the highest mobility and lowest resistivity compared to LSTO on other substrates. The formation of an oxygen-vacancy rich layer near the top region of STO substrate, driven by the growth of an oxide layer at given conditions rather than the growth conditions alone, contributes to the enhanced conductivity of the LSTO/STO heterostructures. Such a surface layer is not achieved by annealing or the growth of an Au layer alone at the same reducing condition. Our work provides an alternative physical origin of STO reduction during thin film growth and the mechanisms on oxygen transfer dynamics revealed here can be applied to design growth and functionalities of other heterostructures.

4. Experimental Section

Pulse laser deposition (PLD) was used to grow epitaxial LSTO thin films with different thicknesses on (001) STO, (110) GdScO₃ (GSO), (001) LAO, (001) LSAT, and CeO₂ buffered (001) STO substrates. To compare the degree of lattice strain of LSTO films on different substrates, XRD and reciprocal space map (RSM) of the films were performed. TEM and HRTEM were used to evaluate the interface and diffraction patterns of 28 and 122 nm LSTO/STO heterostructures. Temperature dependent carrier concentration (n versus T), mobility (μ versus T), and resistivity (ρ versus T) were measured from 10 K to 300 K with a magnetic field of 4 Tesla. Further detailed growth and characterization can be found from the Supporting Information.

Supporting Information

Supporting Information is available from the Wiley Online Library or from the author.

Acknowledgements

Z.C. and H.H.H. contributed equally to this work. The work at Los Alamos National Laboratory was supported by the NNSA's Laboratory Directed Research and Development Program, and Institute of Materials Science and was performed, in part, at the CINT, an Office of Science User Facility operated for the U.S. Department of Energy Office of Science. Los Alamos National Laboratory, an affirmative action equal opportunity employer, is managed by Triad National Security, LLC for the U.S. Department of Energy's NNSA, under contract 89233218CNA000001. The work at the University at Buffalo was partially supported by the U.S. National Science Foundation under award number ECCS-1902623. Q. X. J. also acknowledges the CINT User Program.

Conflict of Interest

The authors declare no conflict of interest.

Data Availability Statement

The data that support the findings of this study are available from the corresponding author upon reasonable request.

Keywords

epitaxial growth, high carrier mobility, oxide heterostructures, oxygen transfer, oxygen vacancy, thin films

Received: October 5, 2021

Revised: November 18, 2021

Published online: January 24, 2022

- [1] A. Chen, Q. Su, H. Han, E. Enriquez, Q. X. Jia, *Adv. Mater.* **2019**, *31*, 1803241.
- [2] D. G. Schlom, L.-Q. Chen, C. J. Fennie, V. Gopalan, D. A. Muller, X. Pan, R. Ramesh, R. Uecker, *MRS Bull.* **2014**, *39*, 118.
- [3] F. Trier, D. V. Christensen, N. Pryds, *J. Phys. D: Appl. Phys.* **2018**, *51*, 293002.
- [4] X. Lu, A. Chen, Y. Luo, P. Lu, Y. Dai, E. Enriquez, P. Dowden, H. Xu, P. G. Kotula, A. K. Azad, D. A. Yarotski, R. P. Prasankumar, A. J. Taylor, J. D. Thompson, Q. X. Jia, *Nano Lett.* **2016**, *16*, 5751.
- [5] S. Gariglio, M. Gabay, J. M. Triscone, *APL Mater.* **2016**, *4*, 060701.
- [6] K. Zou, S. Ismail-Beigi, K. Kisslinger, X. Shen, D. Su, F. J. Walker, C. H. Ahn, *APL Mater.* **2015**, *3*, 036104.
- [7] E. N. Jin, L. Kornblum, D. P. Kumah, K. Zou, C. C. Broadbridge, J. H. Ngai, C. H. Ahn, F. J. Walker, *APL Mater.* **2014**, *2*, 116109.
- [8] J. Biscaras, N. Bergeal, S. Hurand, C. Grossetete, A. Rastogi, R. C. Budhani, D. LeBoeuf, C. Proust, J. Lesueur, *Phys. Rev. Lett.* **2012**, *108*, 247004.
- [9] J. Son, P. Moetafak, J. M. LeBeau, D. Ouellette, L. Balents, S. J. Allen, S. Stemmer, *Appl. Phys. Lett.* **2010**, *96*, 062114.
- [10] J. Biscaras, N. Bergeal, A. Kushwaha, T. Wolf, A. Rastogi, R. C. Budhani, J. Lesueur, *Nat. Commun.* **2010**, *1*, 89.
- [11] S. Okamoto, A. J. Milli, *Nature* **2004**, *428*, 630.
- [12] M. Choi, A. B. Posadas, C. A. Rodriguez, A. O'Hara, H. Seinige, A. J. Kellock, M. M. Frank, M. Tsoi, S. Zollner, V. Narayanan, A. A. Demkov, *J. Appl. Phys.* **2014**, *116*, 043705.
- [13] R. Ghosh, D. Basak, S. Fujihara, *J. Appl. Phys.* **2004**, *96*, 2689.
- [14] F. J. Wong, S.-H. Baek, R. V. Chopdekar, V. V. Mehta, H.-W. Jang, C.-B. Eom, Y. Suzuki, *Phys. Rev. B* **2010**, *81*, 161101.
- [15] W. Siemons, G. Koster, H. Yamamoto, W. A. Harrison, G. Lucovsky, T. H. Geballe, D. H. Blank, M. R. Beasley, *Phys. Rev. Lett.* **2007**, *98*, 196802.
- [16] R. Ohtsuka, M. Matvejeff, K. Nishio, R. Takahashi, M. Lippmaa, *Appl. Phys. Lett.* **2010**, *96*, 192111.
- [17] B. Vilquin, T. Kanki, T. Yanagida, H. Tanaka, T. Kawai, *Appl. Surf. Sci.* **2005**, *244*, 494.
- [18] Z. Q. Liu, W. Lu, S. W. Zeng, J. W. Deng, Z. Huang, C. J. Li, M. Motapothula, W. M. Lü, L. Sun, K. Han, J. Q. Zhong, P. Yang, N. N. Bao, W. Chen, J. S. Chen, Y. P. Feng, J. M. D. Coey, T. Venkatesan, *Adv. Mater. Interfaces* **2014**, *1*, 1400155.
- [19] C. W. Schneider, M. Esposito, I. Marozau, K. Conder, M. Doebeli, Y. Hu, M. Mallepell, A. Wokaun, T. Lippert, *Appl. Phys. Lett.* **2010**, *97*, 192107.
- [20] B. I. Edmondson, S. Liu, S. Lu, H. W. Wu, A. Posadas, D. J. Smith, X. P. A. Gao, A. A. Demkov, J. G. Ekerdt, *J. Appl. Phys.* **2018**, *124*, 185303.
- [21] A. Kalabukhov, R. Gunnarsson, J. Börjesson, E. Olsson, T. Claeson, D. Winkler, *Phys. Rev. B* **2007**, *75*, 121404.
- [22] W. S. Choi, S. Lee, V. R. Cooper, H. N. Lee, *Nano Lett.* **2012**, *12*, 4590.
- [23] B. Vilquin, T. Kanki, T. Yanagida, H. Tanaka, T. Kawai, *Solid State Commun.* **2005**, *136*, 328.
- [24] C. C. Hays, J.-S. Zhou, J. T. Markert, J. B. Goodenough, *Phys. Rev. B* **1999**, *60*, 10367.
- [25] F. V. E. Hensling, C. Xu, F. Gunkel, R. Dittmann, *Sci. Rep.* **2017**, *7*, 39953.
- [26] F. V. E. Hensling, D. J. Keeble, J. Zhu, S. Brose, C. Xu, F. Gunkel, S. Danylyuk, S. S. Nonnenmann, W. Egger, R. Dittmann, *Sci. Rep.* **2018**, *8*, 8846.
- [27] A. Sambri, D. V. Cristensen, F. Trier, Y. Z. Chen, S. Amoroso, N. Pryds, R. Bruzzese, X. Wang, *Appl. Phys. Lett.* **2012**, *100*, 231605.
- [28] K. T. Kang, B. Zhang, Y. Sharma, B. Paudel, H. Wang, P. Dowden, A. Chen, *Appl. Phys. Lett.* **2020**, *117*, 151601.
- [29] A. Spinelli, M. A. Torija, C. Liu, C. Jan, C. Leighton, *Phys. Rev. B* **2010**, *81*, 155110.
- [30] J. S. Kim, S. S. A. Seo, M. F. Chisholm, R. K. Kremer, H. U. Habermeier, B. Keimer, H. N. Lee, *Phys. Rev. B* **2010**, *82*, 201407.
- [31] D. Kan, T. Terashima, R. Kanda, A. Masuno, K. Tanaka, S. Chu, H. Kan, A. Ishizumi, Y. Kanemitsu, Y. Shimakawa, M. Takano, *Nat. Mater.* **2005**, *4*, 816.
- [32] X. Zhou, Z. Liu, *J. Phys. Condens. Matter* **2021**, *33*, 435601.
- [33] T. T. Zhang, C. Y. Gu, Z. W. Mao, X. F. Chen, Z. B. Gu, P. Wang, Y. F. Nie, X. Q. Pan, *Appl. Phys. Lett.* **2019**, *115*, 261604.
- [34] J. E. Sunstrom, S. M. Kauzlarich, P. Klavins, *Chem. Mater* **1992**, *4*, 346.
- [35] L. Fan, X. Gao, D. Lee, E. J. Guo, S. Lee, P. C. Snijders, T. Z. Ward, G. Eres, M. F. Chisholm, H. N. Lee, *Adv. Sci.* **2017**, *4*, 1700045.
- [36] H. H. Sung, J. T. Tsai, C. H. Lin, S. Y. Chen, J. C. Fan, C. R. Lin, *Mater. Sci. Forum* **2011**, *700*, 41.
- [37] Y. Tokura, Y. Taguchi, Y. Okada, Y. Fujishima, T. Arima, K. Kumagai, Y. Iye, *Phys. Rev. Lett.* **1993**, *70*, 2126.
- [38] D. W. Reagor, V. Y. Butko, *Nat. Mater.* **2005**, *4*, 593.
- [39] M. L. Scullin, J. Ravichandran, C. Yu, M. Huijben, J. Seidel, A. Majumdar, R. Ramesh, *Acta Mater.* **2010**, *58*, 457.